Empirical 3D basis for the internal density of a planet

Frédéric Chambat and Yanick Ricard

Laboratoire des Sciences de la Terre, Ecole Normale Supérieure de Lyon, 46 allée d'Italie, F-69364 Lyon,

Cedex 07, France. (fchambat@ens-lyon.fr, ricard@ens-lyon.fr)

SUMMARY

Various papers have discussed the forward relationships between internal density anomalies of a planet and its external gravity field. The inverse modelling, i.e. finding the internal density anomalies from the external potential is known to be highly non unique. In this research note, we explain how a 3D basis can be built to represent the internal density variations which includes a subset that explicitly spans the kernel of the forward gravity operator. This representation clarifies the origin of the non-uniqueness of the gravity sources and implies the existence of a natural minimal-norm inverse for the internal density. We illustrate these ideas by comparing a tomographic model of the mantle to the minimal norm density.

1   INTRODUCTION

A problem in geodynamics is to relate the internal density of a planet to its external gravity field. Classically, the internal density $\rho(r, \theta, \phi)$ and the external gravity potential $V(r, \theta, \phi)$ are both expanded in term of orthogonal functions on the sphere

$$\rho(r, \theta, \phi) = \sum_{l,m} \rho_{lm}(r) Y_{lm}(\theta, \phi), \tag{1}$$

$$V(r, \theta, \phi) = \sum_{lm} V_{lm} \left(\frac{a}{r}\right)^{l+1} Y_{lm}(\theta, \phi), \tag{2}$$

where $Y_{lm}(\theta, \phi)$ are spherical harmonic functions of colatitude θ and longitude ϕ, a is the planetary radius, ρ_{lm} are the spherical components of the density at radius r and V_{lm} the gravity potential coefficients.

We can deduce the coefficients V_{lm} as a function of the density spectral components using

$$V_{lm} = \frac{4\pi G}{a} \int_0^a G_l(r)\, \rho_{lm}(r) r^2 \, dr, \tag{3}$$

where $G_l(r)$ are Green's functions. These Green functions are simply

$$G_l(r) \equiv G_l^S(r) = \frac{1}{2l+1} \left(\frac{r}{a}\right)^l, \tag{4}$$

if we assume that the planet is spherical (hence the superscript 'S'). This Green function implies that shallow mass anomalies are the most efficient to generate gravity potential anomalies (usually represented as geoid undulations).

Of course, a planet is not spherical. To take into account the surface undulation, the density anomalies can be usefully split into internal densities ρ^i and a surface mass $\sigma(\theta, \phi)$. This surface mass with spectral components σ_{lm}, is the product of the topographic height with the density at the Earth's surface. Then, at first order, the external potential verifies

$$V_{lm} = \frac{4\pi G}{a} \int_0^a G_l^S(r)\, \rho_{lm}^i(r) r^2 \, dr + \frac{4\pi Ga}{2l+1} \sigma_{lm}. \tag{5}$$

Internal interfaces can be taken into account in a similar way by introducing equivalent surface mass anomalies, products of the density jumps at these interfaces by their topographies.

At long wavelength, the planets are close to isostatic equilibrium at least for shallow internal mass anomalies. On the Earth, this equilibrium is reached after a time constant of a few thousand years estimated from modelling the pleistocenic glacial unloading (*Cathless* 1975). A simple view of isostasy (see *Dahlen* (1982) for a detailed discussion of the concept of isostasy) indicates that

$$\sigma_{lm} = - \int_{a_i}^a \rho_{lm}^i(r)\, dr, \tag{6}$$

where a_i is a radius below which deviatoric stresses are negligible. By replacing this surface load into the equation eq. (5), we see that we can formally still use eq. (3) where only 'true' internal density are considered (i.e. ρ in eq. (3) is now intended as ρ^i) if we use the new Green function $G_l^I(r)$ where

$$G_l^I(r) = G_l^S(r) - G_l^S(a)\frac{a^2}{r^2} \qquad \text{for r} \geq \text{a}_i. \tag{7}$$

This indicates that shallow mass anomalies (i.e., in the limit $a - r \ll a - a_i$) do not generate geoid undulations. It also predicts that a dense anomaly at depth should be associated with a geoid low. This is in total opposition to the findings obtained for a spherical non-compensated planet (i.e. when eq. (6) is not verified but one imposes $\sigma_{lm} = 0$).

Isostasy is a very good approximation for shallow masses but, of course, compensation departs from isostasy for deep seated masses which means that eq. (6) must be replaced by a more general rule. Various papers (*Ricard et al.* 1984; *Richards and Hager* 1984) have shown that a generalization of the isostatic rule that takes into account sphericity, self-gravitation and the presence of internal interfaces (i.e., the Moho, the Core Mantle Boundary...) can be obtained for a viscous planet with radial rheological properties. In this theory, the topographies involved in the expression of the potential (as in eq. (5)) are computed from the internal density by solving for the mantle flow using a newtonian viscous law with continuities of the velocity, gravity and stress vector at the interfaces. This enables to write V_{lm} in the same way as in eq. (3) with a new Green function $G_l^\eta(r)$ where the superscript reminds that this dynamic compensation model involves the viscosity profile of the mantle η. Using this approach, a good fit to the observed Earth's geoid can been obtained assuming that the internal density of the Earth is related to the observed 3D seismic velocity structure of the mantle (*Forte and Peltier* 1987; *Hager and Clayton* 1989; *Ricard et al.* 1993). Moreover, the geoid, at least at the lowest degrees 2 and 3, is not explained by mass anomalies in the upper mantle since these are compensated by topography anomalies.

Figure 1 depicts the viscous, spherical and isostatic Green functions for degrees 2 and 10. The viscous Green function $G_l^\eta(r)$ shares with the isostatic Green function $G_l^i(r)$ the fact that density anomalies infinitely close to the surface do not generate geoid. Viscous Green functions also vanish at the CMB as mass anomalies near the core are locally compensated by CMB undulations just like shallow mass anomalies are compensated by surface topography. The viscous Green functions have much smaller amplitudes than both spherical and isostatic Green functions. For realistic mantle viscosity profiles, the viscous Green function at $l = 2$ is negative in the lower mantle and positive in the upper mantle. At $l = 10$, the viscous Green function looks like the isostatic Green function for shallow masses, change sign with depth where it becomes somewhat similar to the rigid Green functions.

More general attempts have used 3D viscosity structures (*Zhang and Christensen* 1993) or even have tried to remove the necessity of prescribing a rheology (*Valette and Chambat* 2004). However the most successful explanations of the Earth's geoid are using the simplest model where the rheological properties do not vary laterally.

2   THE INVERSE PROBLEM

It is well known that the inverse gravitational problem, i.e., finding the density structure $\rho(r, \theta, \phi)$ from the gravity coefficients V_{lm} is an ill-posed problem. This means that there is an infinite number of density distributions inside a planet that can produce a given external gravity field. In front of an ill-posed problem two general philosophies can be used. On the one hand, one can make profit of some
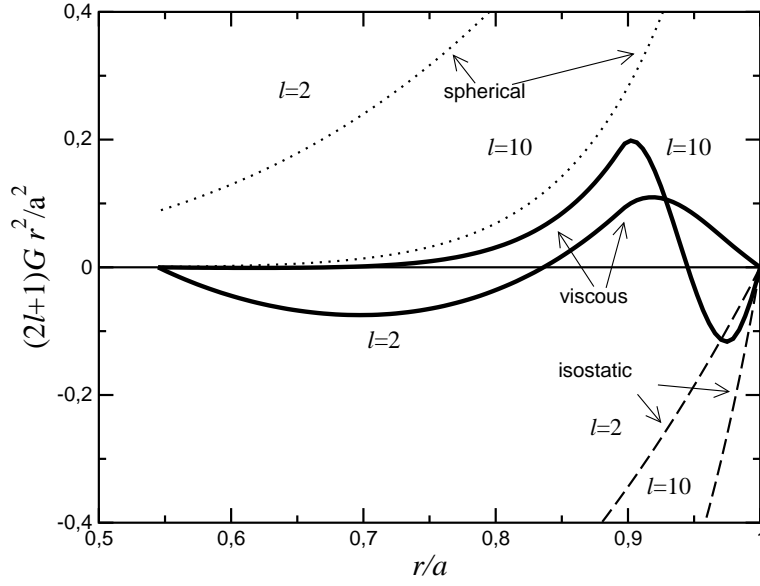
Figure 1. Viscous (thick), spherical (dotted) and isostatic (dashed) Green functions for degrees 2 and 10. The viscous Green function are computed for a model where the lithosphere, the upper mantle, and lower mantle viscosities are proportional to 10, 1 and 30.

a priori knowledge of the density to stabilize the inversion. This can be done for example by assuming that the density remains closely correlated with seismic tomography (this has been used in various papers, see also *Ricard and Wuming* (1991)). On the other hand, one can describe precisely what the null space and what the range of the forward problem are in a Lanczos-type method (*Lanczos* 1961). This was done for a purely spherical planet, i.e., inverting eq. (3) assuming eq. (4), (*Dufour* 1977), but, to our knowledge has never been discussed when the more appropriate $G^\eta(r)$ Green function is used.

This Lanczos-type approach is to built a 3D basis $D_{klm}(r, \theta, \phi)$ to represent the internal structure of a planet (the density, but also the seismic P and S velocities...) in such a way that a subset of this basis is also a basis of the null space of the forward gravity operator.

Let us choose $D_{klm}(r, \theta, \phi) = R_l^k(r)Y_{lm}(\theta, \phi)$, the ortho-normalization of this basis means that

$$\int D_{klm}(r, \theta, \phi)D_{k'l'm'}(r, \theta, \phi) \, dV = 4\pi a^3 \delta_{kk'}\delta_{ll'}\delta_{mm'}, \tag{8}$$

the integral being performed over all the planetary mantle volume (the a^3 term of the right hand side insures that the D_{klm} are dimensionless, the δ is the Kronecker symbol). The spherical harmonics being already orthogonal on the surface of a sphere, we only need to find $R_l^k(r)$ functions so that

$$\int_0^a R_l^k(r)R_l^{k'}(r) \, r^2 \, dr = a^3 \delta_{kk'}. \tag{9}$$

Of course, we can easily take advantage of our understanding of the gravity field of the Earth by

choosing as one of the $R_l^k(r)$ function, the Green function of the gravitational inverse problem $G_l^\eta(r)$. Let us define the norm

$$||R_l^k||^2 = \frac{1}{a^3} \int_0^a R_l^k(r) R_l^k(r) \, r^2 \, dr, \tag{10}$$

and choose

$$R_l^0(r) \equiv \frac{G_l^\eta(r)}{||G_l^\eta||}. \tag{11}$$

Then, the other $R_l^k(r)$ can be constructed by a standard ortho-normalization procedure starting with linearly independent functions. An easy way is to use Chebychev polynomials $T_k(r)$ and define $R_l^k(r)$ as a linear combination of $T_{k-1}(r)$ and of the previous $R_l^{k'}(r)$ $(0 < k' < k)$,

$$R_l^k(r) = \alpha T_{k-1}(r) + \sum_{0 \leq k' < k} \beta_{k'} R_l^{k'}(r), \tag{12}$$

and deduce the constants α and $\beta_{k'}$ from the equations (orthogonality and normalization)

$$\int_0^a R_l^k(r) R_l^{k'}(r) \, r^2 \, dr = 0, \text{ if } 0 \leq k' < k \tag{13}$$

$$||R_l^k(r)|| = 1. \tag{14}$$

Figure 2 depicts the equatorial cross-sections of a few empirical functions for $l = 2$ and $m = 2$. The geoid viscous Green function is computed following *Hager and Clayton* (1989) and using a typical mantle viscosity profile (a lithosphere of thickness 100 km with normalized viscosity 10, an upper mantle of reference viscosity 1, and a lower mantle of normalized viscosity 30). The first empirical function $D_{0,2,2}$ is proportional to this geoid Green function. By construction $D_{0,2,2}$ is the only function that induces a $l = 2$ and $m = 2$ geoid. The other $D_{k,l,m}$ (Figure 2 depicts some of them with $k = 2, 4$ and 6) do not induce any gravity signal outside the planet.

By construction, we can replace eq. (1) by

$$\rho(r, \theta, \phi) = \sum_{k,l,m} \rho_{klm} D_{klm}(r, \theta, \phi), \tag{15}$$

where ρ_{klm} are the components of the density on the empirical basis. This expansion introduced in eq. (3) leads to

$$V_{lm} = 4\pi G a^2 ||G_l^\eta|| \rho_{0lm}, \tag{16}$$

and the solution of minimal norm for the inverse problem is simply

$$\rho^{min}(r, \theta, \phi) = \frac{1}{4\pi G a^2} \sum_{lm} \frac{1}{||G_l^\eta||} V_{lm} D_{0lm}(r, \theta, \phi). \tag{17}$$

This minimal norm solution is of course independent of any radial basis and only depends upon the
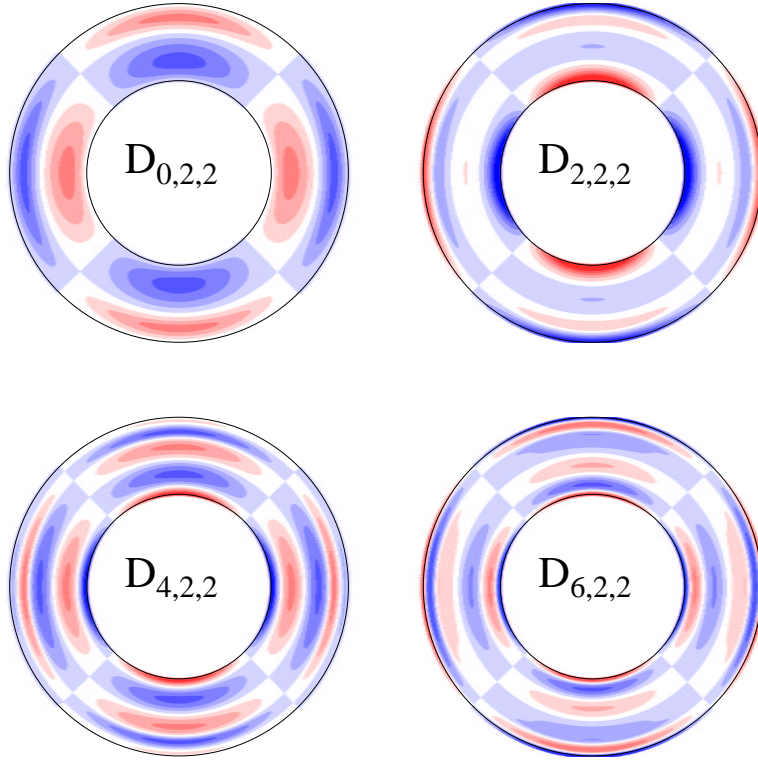
Figure 2. Equatorial cross sections of empirical basis functions for $l = 2$ and $m = 2$. Only the first one ($D_{0,2,2}$, top left) induces an external gravity field. This first function is based on a gravity The other empirical basis functions (e.g., $D_{2,2,2}$, $D_{4,2,2}$ $D_{6,2,2}$) span the kernel of the gravity operator, they do not induce any external gravity field.

Green functions. We can define the radial resolution kernel $R_l(r, r')$ associated with this estimator by

$$\rho_{lm}^{min}(r) = \int_0^a R_l(r, r')\rho_{lm}(r')dr'. \tag{18}$$

By combining the definitions of the minimal density eq. (17) with that of the potential, eq. (5), we obtain

$$R_l(r, r') = \frac{1}{a^3}R_l^0(r)R_l^0(r')r'^2 = \frac{1}{||G_l^\eta||^2 a^3}G_l^\eta(r)G_l^\eta(r')r'^2. \tag{19}$$

As expected this resolution does not depend of the radial basis. At a given r, this resolution is proportional to $G_l^\eta(r')r'^2$ already plotted in Figure 1. A very good resolution would imply that ρ_{lm}^{min} remains close to the actual density ρ_{lm} and therefore that $R_l(r, r')$ is similar to the Dirac function $\delta(r - r')$. This is far from being the case as the resolution of the gravity data is indeed very low.

All the solutions of the inverse gravimetric problem can be obtained by adding any component of the null space which has the form

$$\rho^{null}(r, \theta, \phi) = \sum_{k \neq 0, l, m} n_{klm}D_{klm}(r, \theta, \phi), \tag{20}$$

for any coefficients n_{klm}.

3 APPLICATION

Bearing in mind that the seismic global heterogeneities seen by tomography are more or less proportional to the density anomalies, we project these velocity anomalies onto the D_{0lm} subset to emphasize the heterogeneities that affect Earth's gravity field. To perform this exercise, we use the composite model "Smean" of *Becker and Boschi* (2002) (an average of previous models) that has the advantage of providing at the same time a very good fit to the geoid ($\sim 60\%$ of variance reduction) and be rich in short wavelength anomalies (up to $l = 31$). Alternatively, from the observed geoid, we can easily compute the solution of minimal norm for the density. Of course it does not describe the true density within the Earth but its projection onto the same subset D_{0lm} as the velocity. The results are depicted in Figure 3.

The first row depicts the velocity anomalies at mid upper mantle ((a), left) and mid lower mantle ((b), right). The second row filters out from the components invisible to the external gravity field. This filtering emphasizes the anomalies related to slabs in the upper mantle (c). In the lower mantle (d), only the long wavelength density components affect the external gravity field. These heterogeneities are very close to those predicted from the observed external gravity field (minimal norm density models, bottom row). To have roughly similar color ranges for the velocity maps (top and middle rows) and for the minimal norm density maps (bottom row), the velocity scale varies between ± 40 m s^{-1} and the density scale between ± 12 kg m^{-3}. This suggests throughout the mantle a uniform density/velocity conversion of order 0.3 kg m^3/m s^{-1}. This conversion factor is typically what is predicted from laboratory estimates and other geoid modelling (e.g. *Hager and Clayton* (1989)).

4 CONCLUSIONS

The relationships between the gravity field and the internal structure of the Earth that we have illustrated in this paper, are not new. The forward relations have been known since the eighties (the deep mantle origin of the long wavelength geoid or degree 2-3, the signature of slabs at degrees 4-10) and various papers have performed inverse modelling. More precisely, it is well known that an appropriate velocity/density conversion of the tomographic models provides a good fit of the geoid. Here we show here that, at each depth, the projections of the velocity v_S and the density ρ onto the orthogonal of the gravity null space are proportional. The comparison of the bottom rows of figure 3 shows that the lateral variations at 1800 km are mainly due to the lowest degrees contribution, which is not the case at 500 km. It gives a convincing indication of the deep origin of the geoid at low degrees.
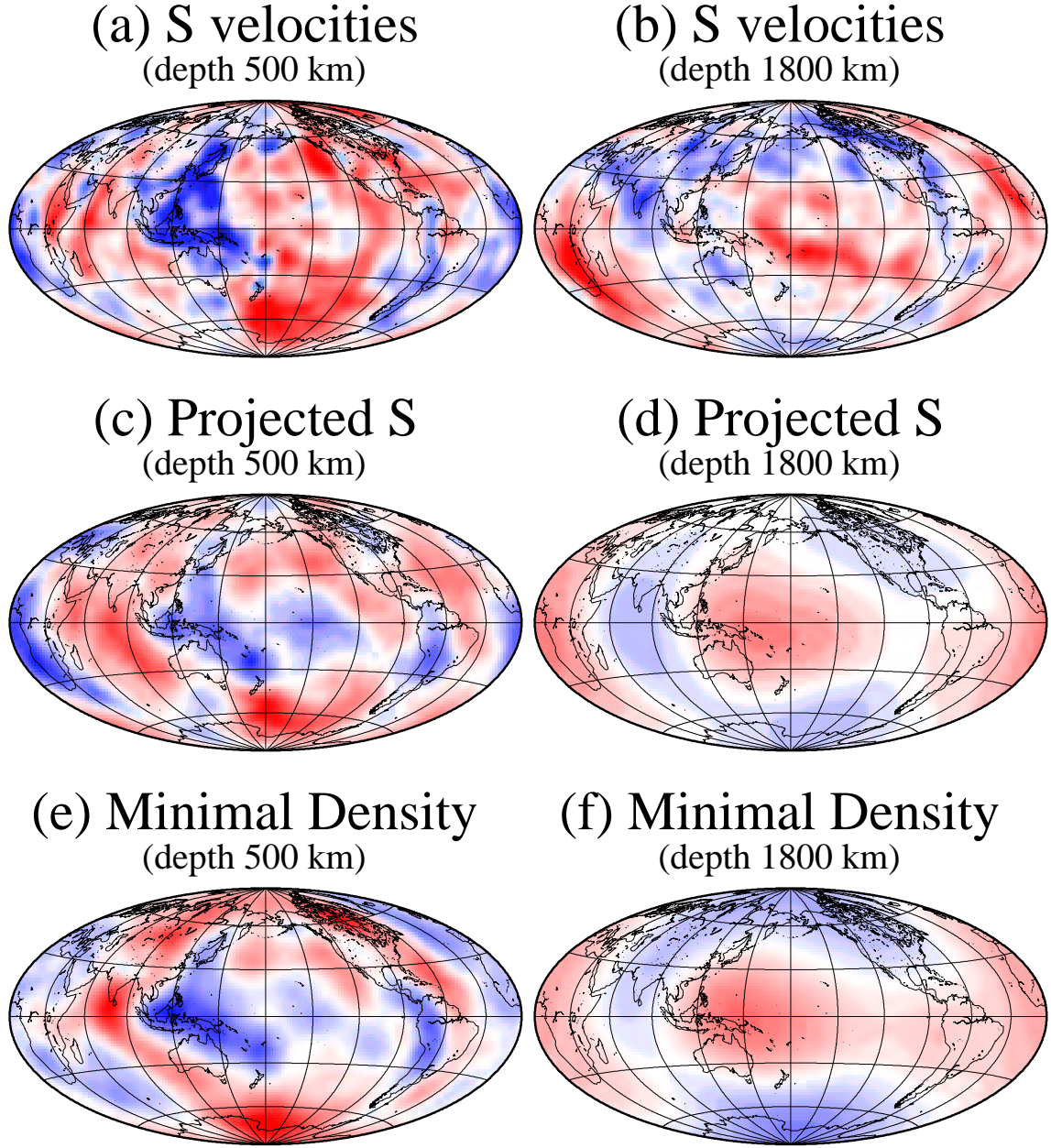
(a) S velocities
(depth 500 km)

(b) S velocities
(depth 1800 km)

(c) Projected S
(depth 500 km)

(d) Projected S
(depth 1800 km)

(e) Minimal Density
(depth 500 km)

(f) Minimal Density
(depth 1800 km)

Figure 3. (a) and (b) Mid upper and mid lower mantle S tomography (Smean model, (*Becker and Boschi* 2002)). (c) and (d) S tomographies filtered out from heterogeneities invisible to the gravity field. (e) and (f) Minimal norm densities predicted from the external gravity field. A same scale is used for the 4 velocity maps (between $\pm$ 40 m s^{-1}). The two density maps vary between $\pm$ 12 kg m^{-3}.

Moreover our approach can be a useful pedagogical way to explain the non-uniqueness of gravity inversion and our radial basis could be used in seismic tomographic inversion in order to explicitly identify the velocity space constrained by the geoid. The description of the internal density of the Earth requires the knowledge of the coefficients ρ_{klm}. A lateral resolution λ_l is attained when all the coefficients up to $l_{max} = |m_{max}| \sim 2\pi a/\lambda_l$ are known. A radial resolution λ_r corresponds to

$k_{max} \sim a/\lambda_r$. From a given model deduced from seismic modelling and complete up to k_{max} and l_{max}, i.e. having $k_{max}(l_{max}+1)^2$ terms, a subset of dimension k_{max} could have been deduced directly from the gravity field (assuming that the relationship between velocities and densities are known, and that the viscosity is only depth dependent). This shows at the same time the potentiality and the low resolution power of gravity.

ACKNOWLEDGMENTS

REFERENCES

Becker, T. W., and L. Boschi, 2002. A comparison of tomographic and geodynamic mantle models, *Geochem. Geophys. Geosyst.*, **3**, 2001GC000,168.

Cathless, L. M., *The viscosity of the Earth's Mantle*, University Press Princeton, N.J., 1975.

Dahlen, T., 1982. Isostatic geoid anomalies on a sphere, *J. Geophys. Res.*, **87**, 3943–3947.

Dufour, A. M., 1977. Fonctions orthogonales dans la sphère, résolution théorique du problème du potentiel terrestre, *Bull. Geod.*, **51**, 227–237.

Forte, A. M., and W. R. Peltier, 1987. Plate tectonics and aspherical Earth structure: the importance of poloidal-toroidal coupling, *J. Geophys. Res.*, **92**, 3645–3679.

Hager, B. H., and R. W. Clayton, Constraints on the structure of mantle convection using seismic observations, flow models, and the geoid, in *Mantle Convection*, edited by W. R. Peltier, pp. 657–764, Gordon and Breach New York, 1989.

Lanczos, C., *Linear Differential Operators*, Van Nostrand, London, 1961.

Ricard, Y., and B. Wuming, 1991. Inferring the viscosity and the 3d structure of the mantle from geoid, topography and plate velocities, *Geophys. J. Int.*, **105**, 561–571.

Ricard, Y., L. Fleitout, and C. Froidevaux, 1984. Geoid heights and lithospheric stresses for a dynamic Earth, *Ann. Geophysica*, **2**, 267–286.

Ricard, Y., M. A. Richards, C. Lithgow-Bertelloni, and Y. Le Stunff, 1993. A geodynamic model of mass heterogeneity, *J. Geophys. Res.*, **98**, 21,895–21,909.

Richards, M. A., and B. H. Hager, 1984. Geoid anomalies in a dynamic Earth, *J. Geophys. Res.*, **89**, 5987–6002.

Valette, B., and F. Chambat, Relating gravity, density, topography and state of stress inside a planet, in V^{th} *Hotine-Marussi Symposium on Mathematical Geodesy, IAG Symposium Series, vol 117*, edited by F. Sanso, Springer, Berlin & Heidelberg, 2004.

Zhang, S., and U. Christensen, 1993. The effect of lateral viscosity variations on geoid, topography and plate motions induced by density anomalies in the mantle, *Geophys. J. Int.*, **114**, 531–547.